Mechanical and oxidation behavior of textured Ti_2AlC and Ti_3AlC_2 MAX phase materials

Xiaoqiang Li[a,1,*], Xi Xie[b,1], Jesus Gonzalez-Julian[a], Jürgen Malzbender[a], Rui Yang[b,**]

1 The two authors contributed equally to this paper

a Forschungszentrum Jülich GmbH, Institute of Energy and Climate Research (IEK), 52425 Jülich, Germany.

b Institute of Metal Research, Chinese Academy of Sciences, 110016 Shenyang , China

* Corresponding author, e-mail: Xiaoqiang Li, xi.li@fz-juelich.de

** Corresponding author, e-mail: Rui Yang, ryang@imr.ac.cn

Abstract

Highly textured Ti_2AlC and Ti_3AlC_2 ceramics were successfully fabricated by a two-step fabrication process, and the Lotgering orientation factors for {00*l*} planes of textured Ti_2AlC and Ti_3AlC_2 were calculated as 0.82 and 0.71, respectively. The effect of texturing was evaluated in terms of elastic modulus and hardness by macro- and micro-indentation. Moreover, the oxidation behavior of the MAX phases was investigated at 1300 °C in air, revealing that the oxidation was markedly anisotropic, where the textured side surface exhibited much better oxidation resistance, resulting from the rapid diffusion of Al element within its basal planes to form a protective Al_2O_3 scale on it. Furthermore, Ti_2AlC had larger difference regarding oxidation behavior between the top and side surface than Ti_3AlC_2, correlated to its higher Al ratio, leading to higher texturing degree and more diffusion pathways to the outer surface to produce an Al_2O_3 layer already at the initial oxidation stage.

Keywords: Ti_2AlC; Ti_3AlC_2; Texturing; Mechanical properties; Oxidation.

1. Introduction

Ternary carbide and nitride phases of the structure $M_{n+1}AX_n$ (MAX), where "M" is an early transition element, "A" represents elements of group IIIA to VIA and "X" corresponds to either C or N, and *n* = 1-3, are widely studied due to their promising ambient and high-temperature physical properties, such as high electrical and thermal conductivities, high elastic modulus, excellent machinability, good thermal shock resistance and damage tolerance [1-4]. All MAX phases, at the moment more than 70 different compositions are known, possess a hexagonal crystal structure, where M_6X octahedral interleaved with A-A layers. As a result, metallic and covalent/ionic bondings coexist in the chemical structure, leading to a unique combination of properties. As ceramics, MAX phases have low density, high elastic modulus, and some of them excellent oxidation and corrosion resistance at high temperature, meanwhile as their metallic character they show high electrical and thermal conductivities, good thermal shock resistance and damage tolerance, as well as good machinability [5-8]. Among all the compositions, aluminum based MAX phases present the highest potential due to their excellent oxidation and corrosion resistance at high temperature related to their in-situ formation of an external, protective and well-adhered α-Al_2O_3 layer [9-11]. Ti_2AlC, Ti_3AlC_2, and Cr_2AlC are the most studied MAX phases due to their excellent oxidation resistance under aggressive environmental conditions at temperature between 1000 and 1300 °C [12-13].

Among the Al-based MAX phase ceramics, Ti_2AlC and Ti_3AlC_2 are the most studied compositions and both are composed of the same elements (Ti, Al, C), but with different ratio of the elements, especially for Al. This element is essential for the oxidation performance, thus offering the possibility to investigate the influence of the Al ratio on the mechanical and oxidation behavior. The Al contents are 16.7 at. % and 25 at. % in Ti_3AlC_2 and Ti_2AlC ceramics, respectively. Actually, Ti_2AlC has been continually drawing attention due to its relative lightweight (4.11 g/cm^3), low cost to achieve high purity, and superior oxidation resistance. Consequently it is a very promising material to be operated under corrosive, and high temperature applications such as in nuclear power plants and aircraft engines [14-15].

It is well known that materials with textured microstructure exhibit anisotropic properties, and

may achieve a better response to some conditions than isotropic compounds. This kind of materials plays an important role in various application fields [16-18]. To date, there are some works regarding the fabrication of textured MAX phase ceramics to obtain high strength and toughness simultaneously. In 2004, Murugaiah et al. [19] intended to fabricate textured Ti_3SiC_2 ceramic by tape casting followed by pressureless sintering. The basal plane of the as-obtained polycrystalline Ti_3SiC_2 was parallel to the surface as a result of preferential grain growth. However, the texturing was not homogeneous and the texture degree was low since the Ti_3SiC_2 grains were not aligned to one preferred direction. Using the strong magnetic field alignment (SMFA) method, Hu et al. [20-23] fabricated highly textured Nb_4AlC_3 and Ti_3SiC_2 ceramics. Interestingly the two phases behaved differently under the strong magnetic field (12 T). Whereas the *c*-axis of Nb_4AlC_3 was aligned parallel, that of Ti_3SiC_2 was oriented perpendicular to the magnetic field direction. Another alternative to develop textured MAX phases is the process referenced as edge-free spark plasma sintering (EFSPS), Lapauw et al. [24] successfully fabricated textured Ti_3SiC_2, Ti_3AlC_2 and Ti_2AlC ceramics by this method. However, the orientation factors of these textured ceramics were as low as 0.5. The texturing could be enhanced through the combination of EFSPS with thermal explosion, as developed recently to prepare highly textured Ti_2AlN. The Lotgering orientation factor on the textured top surface (TTS) was 0.80 [25]. In addition, Duan et al. [26] prepared textured Cr_2AlC ceramic through spark plasma sintering (SPS) using crushed and milled pressure-less sintering Cr_2AlC powders with different average grain sizes.

However, the preparation methods of textured MAX phase mentioned above possess some disadvantages such as the complexity and high cost in case of SMFA and EFSPS, as well as the complexity for the fabrication of products with large size via SPS. Therefore, preparing highly textured MAX phase ceramics with high purity and low cost still remains a challenge. Hence, in the current work a simple and more efficient fabrication method is proposed, using hot pressing (HP) sintering to induce grain texture in MAX phases.

Regarding properties, MAX phases possess low hardness and flexural strength, which affects their industrial applications as structural materials [27]. One effective method to reinforce MAX

phases is to add Al_2O_3 particles to increase hardness and strength [28-29]. Besides, alumina particles present remarkable chemical stability in MAX phases and have a compatible thermal expansion coefficient. As reported in the literature, the addition of Al_2O_3 particles improved the mechanical properties and wear resistance of MAX phases [30-32]. Moreover, the reinforcing effect appeared to be more pronounced in case of decreasing the ceramic particle sizes [33].

In this work, coarse grain (CG) Ti_2AlC and Ti_3AlC_2 ceramics were ball milled in oxygen containing atmosphere to in-situ synthesize dispersive Al_2O_3 particles. The textured microstructure was developed in a second step using a HP, leading at the same time to a full densification of the materials [14]. Elastic modulus and micro-hardness were characterized under different loads via micro-indentation, meanwhile the morphologies of the indentations were utilized to assess differences related to the texture. Furthermore, the oxidation behavior at elevated temperatures was characterized. The work serves as a basis for a database on fabrication and mechanical properties of MAX phase material with high texture degree and also compares the physical and oxidation properties of carbide MAX phase ceramics with different aluminum ratio.

2. Experimental procedure

2.1. Fabrication procedure

The fabrication process of textured samples used in the current work was very similar to that reported in [14]. Briefly, as shown in Fig. 1, coarse grained (CG) bulk carbide Ti_2AlC and Ti_3AlC_2 ceramics were first synthesized via hot pressing (HP) using TiAl (99.5 wt.%, -300 mesh) and TiC (99 wt.%, 2-4 μm) powders in a molar ratio of 1:0.95 and 1:1.9, respectively. The HP was carried at a maximal temperature of 1500 °C for 2 h with a heating rate of 10 K/min in vacuum and using a uniaxial pressure of 30 MPa. The as-sintered samples were machined to remove surface contaminants. Then, the highly pure and coarse grained Ti_2AlC and Ti_3AlC_2 samples were ball milled with a speed of 500 r.p.m using Si_3N_4 balls with a diameter of 5 mm and jar for 48 h in dispersant of ethanol under oxygen gas exposure (volume ratio of O_2:Ar = 1:4) in an in-house developed gas reactive ball milling set-up. Afterwards, the slurry was dried in an oven for 2 days to obtain powders. The milled powders were sieved (-200 mesh), and the

submicro-flake MAX phases powders were obtained. A final HP sintering process was performed to densify and rearrange the submicro-flakes with trace amount of additives under vacuum condition for 2 h at 1200 °C with a heating of 10 K/min assisted by a uniaxial pressure of 30 MPa, followed by a cooling rate of 10 K/min till room temperature. The high surface-to-volume ratio of submicro-flakes resulted in an extra driving force to facilitate the diffusion of elements and reduce the sintering temperature [34]. Furthermore, textured top surfaces of the textured samples, perpendicular to the compression direction, are referenced as TTS, and textured side surfaces, parallel to the compression direction, are designated as TSS.

The as-obtained textured Ti_2AlC and Ti_3AlC_2 samples were cut and embedded in water-free epoxy resin, followed by grinding with SiC sandpaper. Polishing was performed with 3 μm and, subsequently 1 μm diamond polishing paste (MetaDi, BUEHLER) with colloidal silica suspension (50 nm Alkaline, CLOEREN TECGNOLOGY GmbH). Polished samples were used for the XRD analysis, microstructural observation, indentation and oxidation testing.

2.2 Vickers indentation

Well polished TTS and TSS specimens of both textured carbide MAX phase ceramics were also characterized with loads ranging from 1 to 10 N with a fixed holding time of 10 s using a Vickers hardness tester (Buehler Micromet 1). After that, the imprints induced via the Vickers indenter were observed in a SEM to characterize the morphology and the diagonal length of the imprints [35].

2.3 Micro-indentation

Indentation tests were conducted using a Fischerscope H100C (Helmut Fischer KG, Sindelfingen) which was equipped with a Vickers tip. Various loads (10, 50, 100, 300, 500, 700, 1000 mN) were applied to investigate the elastic modulus (E) and hardness (H) of bulk textured ceramics on different surfaces (TTS and TSS). At each load, at least 64 indentations were performed to get a representative average and standard deviation. Dwelling time and acquisition rate during the tests were 5 s and 10 Hz, respectively. E and H as a function of load of textured bulk material will be presented to assess any potential variability in mechanical characteristics.

Evaluation is based on the Oliver and Pharr methodology on the basis of the indentation load-displacement curve [36], with a consideration of Poisson's ratio (*v)* of 0.19 [37-38] and 0.20 [39] for Ti_2AlC and Ti_3AlC_2, respectively.

2.4 Thermogravimetric analysis

The dimension of the polished specimens for oxidation testing was $2 \times 4 \times 6$ mm^3. For the TTS-type sample, the pair of TTS surfaces (6×4 mm^2) was orthogonal to the compression direction of hot pressing, corresponding to 54.5 % of the total surfaces area. For the TSS orientation, two pair TSS surfaces (area 6×4 mm^2 and 2×4 mm^2), correspond to 72.7 % of the total area, were tested in a direction transverse to the compression direction. The sample geometry was chosen to avoid delamination (which occurred when thinning the samples) [40].

The oxidation resistance in air was evaluated using a Rigaku Thermo Plus TG8120 TGA machine (Rigaku Corp., Tokyo, Japan) at a maximal temperature of 1300 °C and a heating rate of 5 K/min, then cool down to room temperature with a cooling rate of 5 K/min.

2.5 Microstructural Characterization

Density of the specimens was measured by the Archimedes principle in water at room temperature. The phase compositions within the bulk materials were characterized by X-ray Diffraction (XRD, D8-Discover, Bruker, US) on the polished surface. The microstructure and grain distribution were characterized by field emission scanning electron microscopy (FE-SEM; Zeiss Merlin). The analysis of oxygen concentration was carried out by O/N/H analyzer (LECO TCH600, USA).

3. Results and discussion

SEM images of coarse grain carbide MAX phase powders before and after reactive ball milling process are presented in Fig. 2. The nano-laminated and flake-like structure of the coarse grained MAX phase powders is evident and in subsequent reactive ball milling procedure, the coarse grained MAX phase powders were crushed and the grain size was reduced to less than 1 μm. Additionally, the oxygen content of Ti_2AlC and Ti_3AlC_2 powders before and after the

reactive ball milling were detected to be 0.74 and 5.9 wt. %, 0.75 and 6.0 wt. %, respectively, implying the oxygen was introduced to the MAX phase coarse grain powders during the reactive ball milling.

The XRD patterns of the TTS and TSS surfaces for Ti_2AlC and Ti_3AlC_2 are shown in Fig. 3. For TTS of both textured MAX phase ceramics, the characterized crystal planes are mainly {00*l*} planes, while peak intensities of others are not apparent. This implies that the intensities of {00*l*} planes are much larger than those of {hk0} planes. On the other hand, for TSS, the characteristic peaks of {00*l*} planes are not the only prominent peaks as the {hk0} peaks are increased also strongly. The {hk0} planes are very obvious and steep and the peaks of {hk0} planes are higher than those of {00*l*}. This phenomenon indicates that both Ti_2AlC and Ti_3AlC_2 ceramics show a high orientation concentration along the compression direction and different grain distributions regarding TTS and TSS after hot pressing.

For TTS of the Ti_2AlC ceramics, (002) and (006) planes are the main exposed crystal planes and for Ti_3AlC_2 ceramic, the (002), (004) and (008) planes are the most apparent planes for TTS in the XRD patterns. Particularly, (100) and (110) planes are the dominant peaks in the XRD patterns of Ti_2AlC ceramics for TSS, whereas for TSS of Ti_3AlC_2, the most exposed peaks belong to (100) and (110) planes. Furthermore, diffraction peaks of Al_2O_3 are not detected probably due to its small grain size, relative low quantity, and the overlap with Ti_2AlC and Ti_3AlC_2 peaks. Therefore, its content and grain size are characterized by EBSD below. Qualitatively, the above results support the conclusion that the obtained carbide MAX phase ceramics are textured along the compression direction. In the current work, it is obvious that for the highly textured case, the *c*-axis of both carbide MAX phase grains is close to the compression direction.

Actually, it might be expected that the orientation degree of the textured MAX phase prepared by HP sintering may contribute to a mechanically anisotropic behavior. During the second hot pressing sintering, an unidirectional pressure was applied on the loosely packed MAX phase

flakes, the MAX phase plates rotated and the side with the largest length was deflected to be vertical to compression direction in order to reduce the center of gravity of the powder particles to achieve the final stable stress state to complete the orientation. In addition, since the bonding between the MX and A layers, i.e. Ti_2C or Ti_3C_2 and Al layers, respectively, in the MAX phase crystal structure is relatively weak, shear and delamination along the MX/A interfaces occurs resulting in flake formation might be expected [41-46]. Similar observations have also been reported for graphene and other nano-layered materials prepared under strong shear forces [47-50]. The submicron carbide MAX phase flakes are unconstrained during hot pressing, and the Ti_2C and Ti_3C_2 atom layers in Ti_2AlC and Ti_3AlC_2 grains tend to slip along Al atom layers when a high shear stress is applied. During hot pressing, the carbide MAX phase grains are already exposed to a uniaxial pressure, but actually suffer a complicated micro-scale stress. Regarding the grains in which the *c*-axis which are not parallel to the compression direction, the shear stress along the Al atom layers becomes prominent [25]. Therefore, the slip systems of the MAX phase materials are activated at high temperatures, which leads to the coordinated deformation between the grains during the hot pressing sintering, hence, these grains will start to deform along their {00*l*} planes and the {00*l*} plane of MAX phase materials and rotate to be perpendicular to the compression direction. Moreover, as the grain size of MAX phase ceramics after reactive ball milling are less than 1 μm, which has been verified in Fig. 2, the small grains also result in a tendency to slide, rotate and deform during hot pressing sintering. Therefore, sub-micron Ti_2AlC or Ti_3AlC_2 flakes after reactive ball milling might result in oriented grain growth in this case, which is consistent with EFSPS of highly textured Ti_2AlN [25] and SPS of fine Cr_2AlC powders [26]. Considering the discussion above, as a result, an orientation concentration of Ti_2AlC or Ti_3AlC_2 grains along the compression direction has been achieved via hot pressing. In addition, the Al ratio of Ti_2AlC is larger than that in Ti_3AlC_2, revealing a higher potential for the Ti_2C than Ti_3C_2 atom layers to slide along Al atom layers under a high shear stress, which correspondingly implies a possible higher texture degree of Ti_2AlC.

In order to assess the texture degree of those carbide MAX phase ceramics quantitatively, the

Lotgering orientation factor $f(l)$ is calculated using the equation $f(l)=(P-P_0)/(1-P_0)$ [14, 25]. In the calculation of $f\{00l\}$, P and P_0 are the ratios of $\sum I\{00l\}/\sum I\{hkl\}$ in textured samples and standard JCPDS sample, respectively. While in the calculation of $f\{hk0\}$, P and P_0 are replaced by the ratio of $\sum I\{hk0\}/\sum I\{hkl\}$ correspondingly. $\sum I\{00l\}$, $\sum I\{hk0\}$ and $\sum I\{hkl\}$ are the sums of the peak intensities of the {00*l*), {*hk*0} and {*hkl*} planes from XRD spectra. The JCPDS files used for XRD phase calculation are the following: #29-0095 for Ti_2AlC and #52-0875 for Ti_3AlC_2, respectively.

Based on the XRD patterns, the Lotgering orientation factors of textured Ti_2AlC and Ti_3AlC_2 for {00*l*} planes on TTS are calculated to be 0.82 and 0.71, respectively, suggesting that both textured Ti_2AlC and Ti_3AlC_2 grains have a high orientation along the compression direction. Additionally textured Ti_2AlC grains are more concentrated along the compression direction than textured Ti_3AlC_2 grains in the current study, which is also consistent with the prediction of the texture degree based on the above discussion regarding different Al ratios of Ti_2AlC and Ti_3AlC_2.

Fig. 4 presents SEM images of polished surfaces of the textured Ti_2AlC and Ti_3AlC_2 MAX phase ceramics. The dark phase corresponds to Al_2O_3 particles, whereas the light dark phases to Ti_2AlC or Ti_3AlC_2 grains. It is clear from these images that the textured Ti_2AlC and Ti_3AlC_2 samples obtained at 1200 °C are highly dense without the presence of pores.

In order to illustrate the phase distribution, images of phase mappings of textured Ti_2AlC and Ti_3AlC_2 are shown in Fig. 5. For textured Ti_2AlC and Ti_3AlC_2 ceramics, the Al_2O_3 particles are homogeneously distributed within the carbide MAX phase matrix and trace amounts of impurities remain, such as TiC and TiAl phase. As derived from EBSD, the amounts of different grains are summarized in Table 1, and the overall Al_2O_3 content of textured Ti_2AlC and Ti_3AlC_2 was calculated to be 16.3 and 16.8 wt. % respectively. Moreover, the overall TiAl and TiC of textured Ti_3AlC_2 was characterized to be 0.3 and 11.0 wt. %, respectively. In addition, densities of textured Ti_2AlC and Ti_3AlC_2 are determined via the Archimedes method in water at room

temperature to be 4.08 ±0.01 and 4.15±0.02 g/cm^3, respectively. Correspondingly, the relative densities of textured Ti_2AlC and Ti_3AlC_2 are calculated and summarized in Table 1. It can be clearly seen that the obtained textured Ti_2AlC and Ti_3AlC_2 have really high relative densities, implying a highly dense microstructure, which is also observed in Fig. 4. Note that, the Al_2O_3 content for TTS of textured Ti_2AlC is much higher than that for TSS, which can contribute to the large grain size and some abnormally large Ti_2AlC grains on TTS, as observed in Fig. 6. Furthermore, the large grain size of textured Ti_2AlC for TTS may lead to lower amount of grains that can be detected via EBSD, whereas the grain sizes of Al_2O_3 particles for both MAX phase are almost the same, which is confirmed in Fig. 7. Therefore, the detected Al_2O_3 content on TTS by EBSD for textured Ti_2AlC is larger than the actual value, while that on TSS is closer to the actual derived content due to its relatively small grain size, thus it is possible to compare Al_2O_3 content on TSS of textured Ti_2AlC with that of textured Ti_3AlC_2 due to their similar grain sizes of MAX phase grains. In addition, also the slightly smaller grain sizes of textured Ti_3AlC_2 stem from the larger amount of impurities (TiAl, TiC etc.), which will hinder the grain growth during the sintering. As shown in Fig. 7, the average grain sizes of Al_2O_3 particles are calculated to be about 0.5±0.1 and 0.6±0.2 μm. Additionally, the average grain sizes of TiAl and TiC grains within the Ti_3AlC_2 ceramic are calculated to be 0.5±0.1 and 0.6±0.2 μm, respectively.

Fig. 8 presents EBSD images of polished surfaces of the textured Ti_2AlC and Ti_3AlC_2 ceramics. The areas of light contrast with spindle-shape can be associated with Ti_2AlC or Ti_3AlC_2 grains. Due to the small size, Al_2O_3, TiAl and TiC particles are difficult to assess via XRD and EBSD, hence, it should be noted that the basal plane of most carbide MAX phase grains are almost perpendicular to the compression direction. Furthermore, the grain size of Ti_2AlC and Ti_3AlC_2 for TTS and TSS has an obvious difference, i.e. the grain size of carbide MAX phase on TTS is larger than that on TSS, moreover, the distribution range of grain size on TTS is smaller than that on TSS, which implies the aspect ratio of carbide MAX phase on TTS is smaller than that on TSS.

Fig. 9 presents the distribution of aspect ratios of the carbide MAX phases. The aspect ratio for

TTS is clearly smaller than that for TSS, which fits well with the distribution of grain sizes shown in Fig. 6.

Considering all information presented above, textured Ti_2AlC and Ti_3AlC_2 ceramics have different microstructure for TTS and TSS. In addition, the basal planes of most carbide MAX phase grains are almost perpendicular to the compression direction, manifesting their highly textured nature, which fits well with the high texture degree calculated via the XRD data.

To study the phase structure and grain orientation relationships of textured carbide MAX phases in more detail, the corresponding pole figures of each MAX phase for TTS and TSS are given in Fig. 10. As might be expected, the results from EBSD analysis are in good agreement with the orientation factor calculated from XRD data as well as the EBSD images of polished surfaces, demonstrating also the high texture of obtained textured Ti_2AlC and Ti_3AlC_2 ceramics.

Vickers indentation has been implemented to evaluate the anisotropic mechanical property of the textured carbide MAX phase ceramics, similar to that in [25]. It can be observed that the morphologies of imprints on the TTS and TSS are certainly different. Specifically, all the indentations are square for TTS and rhombic for TSS at all loads ranging from 1 to 10 N. No cracks belonging to a radial or Palmqvist system can be observed even after application of 10 N, implying excellent damage tolerance. In addition, it can be seen that tiny cracks are present around the four corners of indents in case of TTS (Fig. 11(a) and11(c)) after loading to 10 N and that no crack can be observed in case of TSS perpendicular to the compression direction, while at the corners of imprints along the compression direction, delamination and local fracture features are visible.

The Vickers hardness perpendicular to the compression direction (V_1 and V_2) on TTS, and along (P) and perpendicular (V) to the compression direction on TSS for both textured Ti_2AlC and Ti_3AlC_2 are calculated and summarized in Table 2. As shown in Fig. 11, for both textured carbide MAX phase ceramics, the diagonal lengths of the imprints for TTS with both direction perpendicular to the compression direction are almost the same, while for TSS, the diagonal

lengths of the imprints have a large difference in case of the direction perpendicular and parallel to the compression direction (which coincides with the orientation of the *c*-axis texture). As expected, the diagonal length of imprint along the compression direction exceeds diagonal length perpendicular to the compression directions, which can also be clearly seen in Fig. 11. Correspondingly, the Vickers hardness values for TTS are almost the same, while that for TSS along the compression direction is much lower than that with the direction vertical to the compression direction. In addition, the hardness decreases with increase of the applied load. This phenomenon can be attributed to an indentation size effect [51-53].

The differences in indentation impression morphology and hardness values for both indicate a clear relationship between microstructure and anisotropic mechanical property of the textured carbide MAX phase materials. This anisotropic mechanical behavior of the textured carbide MAX phase ceramic is a consequence of their texture.

In order to study the mechanical performance of the textured MAX phase on a microscale level, hardness (*H*) and elastic modulus (*E*) values at different loads (mN) ranging from 10 to 1000 mN (corresponding to different indentation depths) obtained via micro-indentation are measured and respective results are summarized in Table 3. Both parameters decrease slightly with increasing load, especially below 100 mN for *E* and below 300 mN for *H*, which can be related to a larger contribution of grain boundaries at higher loads [54], but for the hardness also to the widely reported indentation size effect [51-53].

It can be seen that the values of hardness on TTS and TSS are approximately the same for both textured carbide MAX phase within the load range from 10 to 1000 mN. On the other hand, the elastic moduli on TSS are significantly larger than that on TTS for both textured carbide MAX phase materials.

Moreover, elastic moduli of textured Ti_2AlC and Ti_3AlC_2 ceramics have a similar tendency regarding applied loads. It has been reported that the elastic moduli of Ti_2AlC and Ti_3AlC_2 are ~ 277 GPa [37-38] and ~ 297 GPa [39], respectively, which are in the middle of the range of

values for TTS and TSS derived from micro-indentation test in the current study. Actually, the differences can be attributed to various factors, such as local porosity and grain boundaries, which might have affected the testing result.

Additionally, owing to the stronger Ti-C bonds compared to Ti-Al bonds in the Ti_2AlC and Ti_3AlC_2 lattice, the Young's modulus perpendicular to *c*-axis is expected to be higher than that along the *c*-axis [22]. The higher Young's modulus perpendicular to *c*-axis is also expected to be beneficial to the motion of phonons along the same direction, therefore, the Young's modulus along the *c*-axis should be lower, according to theoretical calculations, resulting in the weaker resistance against deformation in this direction [25]. Here, the orientation of *c*-axis for the MAX phase grains is close to the compression direction in the current study. Therefore, the elastic moduli on TSS should be larger than that on TTS for both textured carbide MAX phase materials.

In order to investigate the oxidation behavior, the thermogravimetric analysis curves of TTS and TSS for textured carbide MAX phase ceramics are given in Fig. 12. After the TGA tests of the textured carbide MAX phase ceramics at 1300 °C, the mass gains for TTS-type and TSS-type specimens reached 7.9 wt.% and 2.3 wt.%, respectively for textured Ti_2AlC ceramic and 6.8 wt.% and 4.2 wt.%, respectively, for textured Ti_3AlC_2.

Fig. 13 presents optical photographs of the textured samples after thermogravimetric analysis (TGA) test at 1300 °C (dwell time 2 h). It is obvious that for both textured ceramics, the TTS-type surfaces turned yellow, while TSS-type surfaces maintained their starting dark-grey color. The samples exhibited an obvious anisotropic oxidation resistance and TTS surfaces showed serious oxidation. Some yellow phases were produced and attached on the TTS surfaces, while for TSS surfaces for all specimens, there was no obvious oxidation occurring and the initial appearance remained as before TGA test, thus implying basal planes (TTS) showed a reduced oxidation resistance compared to TSS.

Fig. 14 shows the XRD patterns of oxidation products on TTS and TSS for both textured MAX

phase material. As similar to reported work [40], the oxidation products on TTS and TSS sides for both textured MAX phase materials were TiO_2 (rutile), Al_2TiO_5 and Al_2O_3. In addition, the content of these phases was quantified via Rietveld analysis and summarized in Table 4. As expected, the compositions after oxidation on TTS and TSS sides for both textured MAX phase are very similar respectively. Moreover, the amount of Al_2O_3 on TSS is much larger than that on TSS for both textured MAX phase materials, resulting from the thicker Al_2O_3 oxide scale on TSS which protected the surfaces from further oxidation.

In order to gain deeper investigation on the anisotropic oxidation resistance of textured MAX phase materials in the current work, SEM investigations on the cross-sections of TTS and TSS sides, presented in Fig. 15 for both textured MAX phase materials have been also carried out. As expected, similar to photograph of oxidized specimens (Fig. 13), the thickness of oxide scale on TTS is larger than that on TSS side for each textured carbide MAX phase.

In addition, since the microstructure of oxide scale of Ti_2AlC and Ti_3AlC_2 are almost the same as presented in Fig. 15(a-b), the Ti_3AlC_2 material was used for further characterization. After the TGA test at 1300 °C (dwell time 2 h), a non-adherent and passivating oxide scale consisting of Al_2O_3, Al_2TiO_5 and TiO_2 formed on TTS, which was confirmed by energy dispersive spectroscopy (EDS) results in Fig. 15, and the oxidation damage resulted in open pores within the oxidation scales as presented in Fig. 15(c-e). Typically, based on the SEM images on the cross-section, the thickness of oxide scale on TTS for textured Ti_3AlC_2 were measured to be approx. 300 μm , which is much larger than those on TSS (~6 μm) after TGA tests. The thicker oxide scale on TTS than on TSS for both textured MAX phase materials contributed to thicker Al_2O_3 oxide scale on TSS which protected the surfaces from further oxidation, demonstrating the obvious anisotropic oxidation behavior of both textured MAX phase.

Regarding TSS side, a well adherent dense alumina scale covered the TSS as observed in Fig. 15(f). The corresponding analysis of energy dispersive spectroscopy (EDS) and elementary distribution mapping also confirmed the formation of a dense Al_2O_3 scale and small amount of Al_2TiO_5 and TiO_2 comparing to oxide products on TTS. For both TTS and TSS sides, alumina

scale was effective to passivate the material and its disappearance resulted from the reaction between Al_2O_3 and TiO_2 [40].

In summary, there are several noticeable phenomena. First, the mass gains of TTS-type and TSS-type specimens for each textured Ti_2AlC and Ti_3AlC_2 are significantly different. The mass gain of TTS-type samples is much larger than that of TSS-type samples. Moreover, after oxidation for 2 h at 1300 °C, the final weight gains of TTS-type samples for textured Ti_2AlC and Ti_3AlC_2 ceramics are calculated to be 32 and 22 mg/cm^2, respectively, while for TSS-type samples for both carbide MAX phase, the final weight gains for textured Ti_2AlC and Ti_3AlC_2 were -6 and 3 mg/cm^2, respectively. Note that, the negative weight gain (-6 mg/cm^2) of TSS-type samples for textured Ti_2AlC is a result of spallation of the layer which can be observed in Fig. 12. Regarding the mass gain difference of the TTS- and TSS-type specimens for each MAX phase ceramic, it has to be considered that there are a different number of exposed TTS surfaces due to the textured structure, i.e. the grains for TTS of both textured Ti_2AlC and Ti_3AlC_2 ceramics mainly belong to {00*l*} planes, while for TSS, most grains are on {hk0} planes. Additionally, the TTS are mainly composed of MX layers, i.e. Ti_2C and Ti_3C_2 layers, while TSS contains mixed MX layers and A-A atom layers, i.e. Al-Al layers, which join the MX layers within MAX phase lattice, thus the TTS and TSS for each textured carbide MAX phase contain different aluminum composition. Furthermore, the Al layers with their edge exposed on the TSS can be regarded as an element essential with respect to the oxidation resistant alumina layer for MAX phase ceramics, i.e. the rapid outward diffusion of Al atoms on the basal planes forms a protective Al_2O_3 scale [40]. Therefore, TSS will be protected by dense Al_2O_3 layers at the initial oxidation stage, while TTS will be seriously oxidized because of the lack of Al elements and the sluggish diffusion of Al atoms which have to penetrate the MX layers during the oxidation process.

Second, the mass gain on TTS for textured Ti_2AlC (7.9 wt. %) is larger than that of textured Ti_3AlC_2 (6.9 wt. %). On the contrary, the mass gain on TSS-type specimen for textured Ti_2AlC (2.3 wt. %) is less than that for textured Ti_3AlC_2 (4.2 wt. %). As a result, the ratios of weight gains for TTS-type to TSS-type for textured Ti_2AlC and Ti_3AlC_2 are 3.4 and 1.6, respectively.

The much larger difference of the ratio of weight gain of TTS- to TSS-type specimens for textured Ti_2AlC also demonstrates the effect of the higher texture degree and more obvious anisotropic oxidation performance than existing in the case of textured Ti_3AlC_2. The different oxidation behavior may result from the different aluminum content within those two carbide MAX phase ceramics, and there are two factors that influence microstructure and oxidation behavior. First, as discussed above, the Al ratio of Ti_2AlC is larger than that of Ti_3AlC_2, revealing the higher possibilities for the Ti_2C and T_3C_2 atom layers to slide along Al atom layers under a high shear stress, resulting in the possible higher texture degree of Ti_2AlC MAX phase, being confirmed by the Lotgering factor calculated by the XRD data, therefore, the Ti_2C layers and Al atoms layers are more concentrated on the TTS and TSS surfaces, respectively, for textured Ti_2AlC, compared to the existence of Ti_3C_2 layers and Al atoms for textured Ti_3AlC_2. Second, the larger Al ratio within textured Ti_2AlC will provide more access and/or possibilities to diffuse to the outer surface to produce Al_2O_3 layer at the initial oxidation stage. Therefore, the above discussion also implies that the anisotropic oxidation behavior of textured Ti_2AlC should be much more obvious than that of textured Ti_3AlC_2..

4. Conclusion

Textured Ti_2AlC and Ti_3AlC_2 MAX phase ceramics have been successfully fabricated via a two-step fabrication. The coarse grain bulk of carbide MAX phases have been first synthesized via hot pressing, then crushed into sub-micron flakes. Second, the flakes are hot pressed again at 1200 °C with a load of 30 MPa. Resulting {00*l*} planes of textured Ti_2AlC and Ti_3AlC_2 ceramics are highly oriented and vertical to the compression direction. On the basis of XRD data, the Lotgering orientation factors of textured Ti_2AlC and Ti_3AlC_2 ceramics for {00*l*} planes on TTS are calculated to be 0.82 and 0.71, respectively, suggesting that both carbide MAX phase ceramics are highly textured and Ti_2AlC grains are more concentrated along the compression direction than Ti_3AlC_2 grains in current study for the materials with the similar grain sizes.

Regarding Vickers indentations on textured Ti_2AlC and Ti_3AlC_2 ceramics, the diagonal lengths of the imprints on TTS with both directions perpendicular to the compression direction are

almost the same, while on TSS, the diagonal length of indent along the compression direction exceeds the diagonal length perpendicular to the compression direction. The different imprints morphologies for TTS and TSS for both textured carbide MAX phase ceramics are clearly related to an anisotropic response due to the high texture. In addition, the elastic moduli of textured Ti_2AlC and Ti_3AlC_2 present a similar tendency in their load dependencies within loads ranging from 10 to 1000 mN. Additionally, since the Ti-C bonds are stronger than the Ti-Al bonds in the Ti_2AlC and Ti_3AlC_2 lattice, the elastic modulus perpendicular to the *c*-axis is higher than that along the *c*-axis, which also means elastic modulus on TSS is higher than that on TTS for both textured carbide MAX phase materials.

Regarding oxidation behavior, both textured samples exhibited an obvious similar anisotropic oxidation resistance and basal planes (TTS) showed a more pronounced oxidation and hence reduced resistance compared to TSS at 1300 °C. Regarding both textured MAX phase materials, a non-adherent and passivating oxide scale with porous structure consisting of Al_2O_3, Al_2TiO_5 and TiO_2 formed on TTS and a dense alumina scale adhered on TSS side. The oxide scale on TTS is thicker than on TSS for each textured carbide MAX phase as a consequence of obvious texture. The higher oxidation rate of textured Ti_2AlC ceramic can be associated with the higher Al content within Ti_2AlC grains of the lattice, leading to the higher texture degree as well as the possibility for rapid diffusion of aluminum to the outer surface layer to form a protective Al_2O_3 layer.

This work provides a new method to fabricate highly textured carbide MAX phase materials by HP sintering, hence, offering a simple and low-cost route for fabricating highly textured MAX phases with excellent physical and mechanical performance. In addition, the anisotropic mechanical and oxidation behavior of both textured carbide MAX phase ceramics have been investigated and compared. The higher Al content of textured Ti_2AlC ceramic results in a higher texture as well as more access and/or possibilities for diffusion to the outer surface to produce Al_2O_3 layer at the initial oxidation stage, implying the significance of the Al ratio for high texture and oxidation resistance of carbide MAX phases that are composed of the same elements. It provides a guideline for selection and an important factor for a MAX phase as the

potential structural material with excellent oxidation resistance.

Acknowledgements

The authors would like to thank Dr. E. Wessel, Dr. D. Grüner for the microstructural investigations via SEM, and Mr. M. Ziegner for supporting the work with XRD investigations. Supports from Prof. Dr. L. Singheiser, Prof. M. Krüger and Prof. R. Schwaiger are highly acknowledged. Mr. X. Li gratefully acknowledges the support from the China Scholarship Council of China. Prof. J. Gonzalez-Julian thanks the financial support by the Germany's Federal Ministry of Education and Research ("Bundesministerium für Bildung und Forschung") under the MAXCOM project (03SF0534).

References:

[1] M.W. Barsoum, T. El-Raghy, Synthesis and characterization of a remarkable ceramic: Ti_3SiC_2, J. Am. Ceram. Soc. 79 (1996) 1953-1956.

[2] Y.C. Zhou, Z.M. Sun, Microstructure and mechanism of damage tolerance for Ti_3SiC_2 bulk ceramics, Mater. Res. Innovat. 2 (1999) 360.

[3] M.W. Barsoum, The $M_{n+1}AX_n$ phases: a new class of solids; thermodynamically stable nanolaminates, Prog. Solid. State. Chem. 28 (2000) 201-281.

[4] Z.M. Sun, Progress in research and development on MAX phases: a family of layered ternary compounds, Int. Mater. Rev. 56 (2011) 143-166.

[5] C.F. Hu, F.Z. Li, J. Zhang, J.M. Wang, J.Y. Wang, Y.C. Zhou, Nb_4AlC_3: a new compound belonging to the MAX phases, Scr. Mater. 57 (2007) 893-896.

[6] N.J. Lane, M. Naguib, J. Lu, L. Hultman, M.W. Barsoum, Structure of a new bulk $Ti_5Al_2C_3$ MAX phase produced by the topotactic transformation of Ti_2AlC, J. Eur. Ceram. Soc. 32 (2012) 3485-3491.

[7] B. Anasori, J. Halim, J. Lu, C.A. Voigt, L. Hultman, M.W. Barsoum, Mo_2TiAlC_2: a new ordered layered ternary carbide, Scr. Mater. 101 (2015) 5-7.

[8] S. Lu, X.Q. Li, Y.F. Zhou, W.T. Xu, J. W. Pan, Synthesis and mechanical properties of TiB_2/Ti_2AlN composites fabricated by hot pressing sintering, J. Ceram. Soc. Jan. 126 (11) (2018) 900-905.

[9] A.S. Farle, C. Kwakernaak, Svd. Zwaag, W.G. Sloof, A conceptual study into the potential of $M_{n+1}AX_n$-phase ceramics for self-healing of crack damage, J. Eur. Ceram. Soc. 35 (2015) 37-45.

[10] H.J. Yang, Y.T. Pei, J.C. Rao, J.Th.M. De Hosson, S.B. Li, G.M. Song, High temperature healing of Ti_2AlC: On the origin of inhomogeneous oxide scale, Scr. Mater. 65 (2011) 135-138.

[11] B. Cui , R. Sa, D.D. Jayaseelan, F. Inam, M.J. Reece, W. E. Lee, Microstructural evolution during high-temperature oxidation of spark plasma sintered Ti_2AlN ceramics, Acta Mater 60 (2012) 1079-1092.

[12] J.L. Smialek, Kinetic Aspects of Ti_2AlC MAX Phase Oxidation, Oxid. Met. 83 (2015) 351.

[13] J. Gonzalez-Julian, T. Go, D.E. Mack, R. Vaßen, Environmental resistance of Cr_2AlC MAX phase under thermal gradient loading using a burner rig, J. Am. Ceram. Soc. 101 (2018)

1841-1846.

[14] X. Xie, R.Yang, Y.Y. Cui, Q. Jia, C.G. Bai, Fabrication of textured Ti_2AlC lamellar composites with improved mechanical properties, J. Mater. Sci. Technol. 38 (2020) 86-92.

[15] Y.C. Zhou, X.H. Wang, Z.M. Sun, S.Q. Chen, Electronic and structural properties of the layered ternary carbide Ti_3AlC_2, J. Mater. Chem. 11 (2001) 2335-2339.

[16] H.R. Wenk, P. Van Houtte, Texture and anisotropy, Rep. Prog. Phys. 67 (2004) 1367-1428.

[17] M. Wei, D. Zhi, D.G. Brandon, Oxide ceramic laminates with highly textured α-alumina interlayers: I. Texture control and laminate formation, J. Mater. Sci. 41 (2006) 7425-7436.

[18] H.T. Zhang, H.X. Yan, X.D. Zhang, M.J. Reece, J. Liu, Z.J. Shen, Y.M. Kan, P.L. Wang, The effect of texture on the properties of $Bi_{3.15}Nd_{0.85}Ti_3O_{12}$ ceramics prepared by spark plasma sintering, Mater. Sci. Eng., B 475 (2008) 92-95.

[19] A. Murugaiah, A. Souchet, T. El-Raghy, M. Radovic, M. Sundberg, M.W. Barsoum, Tape Casting, Pressureless Sintering, and Grain Growth in Ti_3SiC_2 Compacts, J. Am. Ceram. Soc. 87 (2004) 550-556.

[20] C.F. Hu, Y. Sakka, H. Tanaka, T. Nishimura, S. Grasso, Fabrication of Textured Nb_4AlC_3 Ceramic by Slip Casting in a Strong Magnetic Field and Spark Plasma Sintering, J. Am. Ceram. Soc. 94 (2011) 410-415.

[21] C.F. Hu, Y. Sakka, S. Grasso, T. Suzuki, H. Tanaka, Tailoring Ti_3SiC_2 Ceramic via a Strong Magnetic Field Alignment Method Followed by Spark Plasma Sintering, J. Am. Ceram. Soc. 94 (2011) 742-748.

[22] C.F. Hu, Y. Sakka, T. Nishimura, S.Q. Guo, S. Grasso, H. Tanaka, Physical and mechanical properties of highly textured polycrystalline Nb_4AlC_3 ceramic, Sci. Technol. Adv. Mater. 12 (2011) 044603.

[23] C.F. Hu, Y. Sakka, S. Grasso, T. Nishimura, S.Q. Guo, H. Tanaka, Shell-like nanolayered Nb_4AlC_3 ceramic with high strength and toughness, Scr. Mater. 64 (2011) 765-768.

[24] T. Lapauw, K. Vanmeensel, K. Lambrinou, J. Vleugels, A new method to texture dense $M_{n+1}AX_n$ ceramics by spark plasma deformation, Scr. Mater. 111 (2016) 98-101.

[25] Y. Liu, Y.X. Li, F. Li, H. Cui, Y.P Pu, S.W. Guo, Z.Q. Shi, Highly textured Ti_2AlN ceramic prepared via thermal explosion followed by edge-free spark plasma sintering, Scr. Mater. 136 (2017) 55-58.

[26] X. Duan, L. Shen, D. Jia, Y. Zhou, S. van der Zwaag, W.G. Sloof, Synthesis of high-purity, isotropic or textured Cr_2AlC bulk ceramics by spark plasma sintering of pressure-less sintered powders, J. Eur. Ceram. Soc. 35 (2015) 1393-1400

[27] J.X. Chen, Y.C. Zhou, Strengthening of Ti_3AlC_2 by incorporation of Al_2O_3, Scr. Mater. 50 (2004) 897-901.

[28] Y.M. Luo, S.Q. Li, J. Chen, R.G. Wang, J.Q. Li, W. Pan, Effect of composition on properties of alumina/titanium silicon carbide composites, J. Am. Ceram. Soc. 85 (2002) 3099-3101.

[29] H.J. Wang, Z.H. Jin, Y. Miyamoto, Effect of Al_2O_3 on mechanical properties of Ti_3SiC_2/Al_2O_3 composite, Ceram. Int. 28 (2002) 931-934.

[30] A.J. Li, Y.C. Zhou, A Novel Method to Make Tough Ti_2AlC/Al_2O_3- and Ti_3AlC_2/Al_2O_3-Laminated Composites, J. Am. Ceram. Soc. 93 (2010) 4110-4114.

[31] C.L. Yeh, C.W. Kuo, Y.C. Chu, Formation of Ti_3AlC_2/Al_2O_3 and Ti_2AlC/Al_2O_3 composites by combustion synthesis in Ti-Al-C-TiO_2 systems, J. Alloys. Compd. 494 (2010) 132-136.

[32] M. Zarezadeh Mehrizi, R. Beygi, Direct synthesis of Ti_3AlC_2-Al_2O_3 nanocomposite by mechanical alloying, J. Alloys. Compd. 740 (2018) 118-123.

[33] D. Gu, G. Meng, C. Li, W. Meiners, R. Poprawe, Selective laser melting of TiC/Ti bulk nanocomposites: Influence of nanoscale reinforcement, Scr. Mater. 67 (2012) 185-188.

[34] H.Z. Guo, A. Baker, J. Guo, C.A. Randall, Protocol for Ultralow-Temperature Ceramic Sintering: An Integration of Nanotechnology and the Cold Sintering Process, ACS. Nano. 10 (11) (2016) 10606-10614.

[35] ASTM E384-17, Standard Test Method for Microindentation Hardness of Materials, ASTM International, West Conshohocken, PA, (2017).

[36] W.C. Oliver, G.M. Pharr, An improved technique for determining hardness and elastic modulus using load and displacement sensing indentation experiments, J. Mater. Res. 7 (2011) 1564-1583.

[37] B. Manoun, S.K. Saxena, M.W. Barsoum, T. El-Raghy, X-ray high-pressure study of Ti_2AlN and Ti_2AlC, J. Phys. Chem. Solids. 67 (2006) 2091-94.

[38] M. Radovic, A. Ganguly, M.W. Barsoum, T. Zhen, P. Finkel, S.R. Kalidindib, E. Lara-Curzioa, On the elastic properties and mechanical damping of Ti_3SiC_2, Ti_3GeC_2, $Ti_3Si_{0.5}Al_{0.5}C_2$

and Ti_2AlC in the 300-1573 K temperature range, Acta Mater. 54 (2006) 2757-67.

[39] B. Manoun, S.K. Saxena, G. Hug, A. Ganguly, E.N. Hoffman, M.W. Barsoum, Synthesis and compressibility of $Ti_3(Al_{1.0}Sn_{0.2})C_2$ and $Ti_3Al(C_{0.5},N_{0.5})_2$, J. Appl. Phys. 101 (2007) 113523.

[40] L.D. Xu, D.G. Zhu, Y.L. Liu, T.S. Suzuki , B.N Kim, Y. Sakka, S. Grasso, C.F. Hu, Effect of texture on oxidation resistance of Ti_3AlC_2, J. Eur. Ceram. Soc. 38 (2018) 3417-3423.

[41] X.H. Wang, Y.C. Zhou, Layered Machinable and Electrically Conductive Ti_2AlC and Ti_3AlC_2 Ceramics: a Review, J. Mater. Sci. Technol. 26 (5) (2010) 385-416.

[42] S.B. Li, W.H. Xiang, H.X. Zhai, Y. Zhou, C.W. Li, Z.L. Zhang, Formation of a single-phase Ti_3AlC_2 from a mixture of Ti, Al and TiC powders with Sn as an additive, Mater. Res. Bull. 43 (8-9) (2008) 2092-2099.

[43] X.L. Hong, B.C. Mei, J.Q. Zhu, W.B. Zhou, Fabrication of Ti_2AIC by hot pressing of Ti, TiC, Al and active carbon powder mixtures, J. Mater. Sci. 39 (2004) 1589-1592.

[44] G.P. Bei, B.J. Pedimonte, T. Fey, P. Greil, Oxidation Behavior of MAX Phase $Ti_2Al_{(1-x)}Sn_xC$ Solid Solution, J. Am. Ceram. Soc. 96 (5) (2013) 1359-1362.

[45] O. Mashtalir, M. Naguib, V.N. Mochalin, Y. Dall'Agnese, M. Heon, M.W. Barsoum, Y. Gogotsi, Intercalation and delamination of layered carbides and carbonitrides, Nat. Commun. 4 (2013) 1-7.

[46] X.D. Zhang, J.G. Xu, H. Wang, J.J. Zhang, H.B. Yan, B.C. Pan, J.F. Zhou, Y. Xie, Ultrathin nanosheets of MAX phases with enhanced thermal and mechanical properties in polymeric compositions: $Ti_3Si_{0.75}Al_{0.25}C_2$, Angew. Chem. Int. Ed. 52 (2013) 4361-5.

[47] Y.C. Fan, L.J. Wang, J.L. Li, J.Q. Li, S.K. Sun, F. Chen, L.D. Chen, W. Jiang, Preparation and electrical properties of graphene nanosheet/Al_2O_3 composites, Carbon 48 (2010) 1743-9.

[48] L.H. Li, Y. Chen, G. Behan, H.Z. Zhang, M. Petravic, A.M. Glushenkov, Large-scale mechanical peeling of boron nitride nanosheets by low-energy ball milling, J. Mater. Chem. 21 (2011) 11862-6.

[49] H. Porwal, S. Grasso, M. Reece M, Review of graphene-ceramic matrix composites, Adv. Appl. Ceram. 112 (2013) 443-54.

[50] Y.G. Yao, Z.Y. Lin, Z. Li, X.J. Song, K.S. Moon, C.P. Wong, Large-scale production of two-dimensional nanosheets, J. Mater. Chem. 22 (2012) 13494-9.

[51] J.H. Gong, J.J. Wu, Z.D. Guan, Analysis of the indentation size effect on the apparent

hardness for ceramics, Mater. Lett. 38 (3) (1999) 197-201.

[52] A.A. Elmustafa, D.S. Stone. Nano-indentation and the indentation size effect: Kinetics of deformation and strain gradient plasticity, J. Mech. Phys. Solids. 51 (2) (2003) 357-381.

[53] S.J. Bull, T.F. Page, E.H. Yoffe, An explanation of the indentation size effect in ceramics, Phil. Mag. Lett. 59 (6) (1989) 281-288.

[54] J.F. Nonemacher, S. Naqash, F. Tietz, J. Malzbender, Micromechanical assessment of Al/Y-substituted NASICON solid electrolytes, Ceram. Int. 45 (17) (2019) 21308-21314.

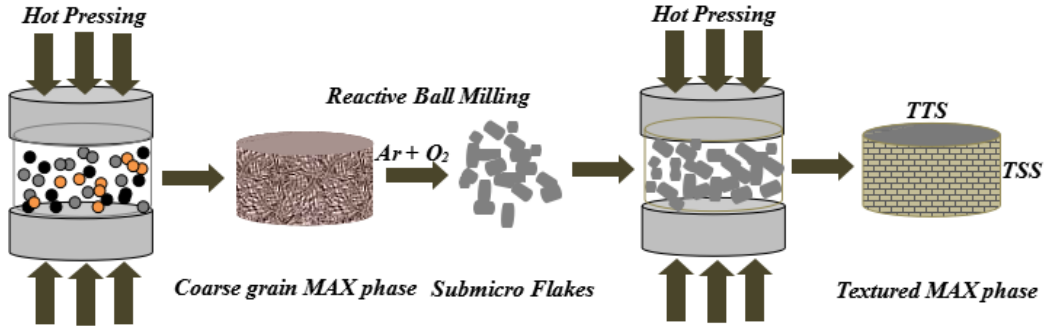

Fig. 1 The schematic illustraton of the fabrication prcedure for textured carbide MAX phase.

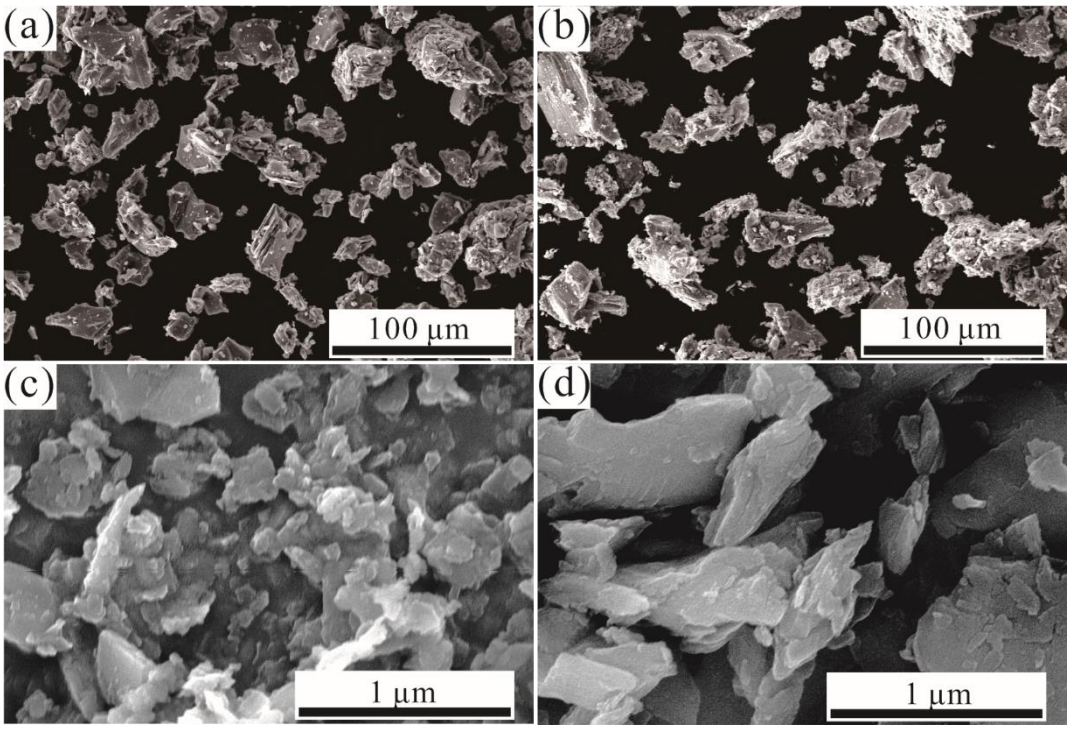

Fig. 2 The SEM images of coarse grain (a) Ti_2AlC; (b) Ti_3AlC_2 powder and corresponding (c) Ti_2AlC and (d) Ti_3AlC_2 powder after reactive balling milling.

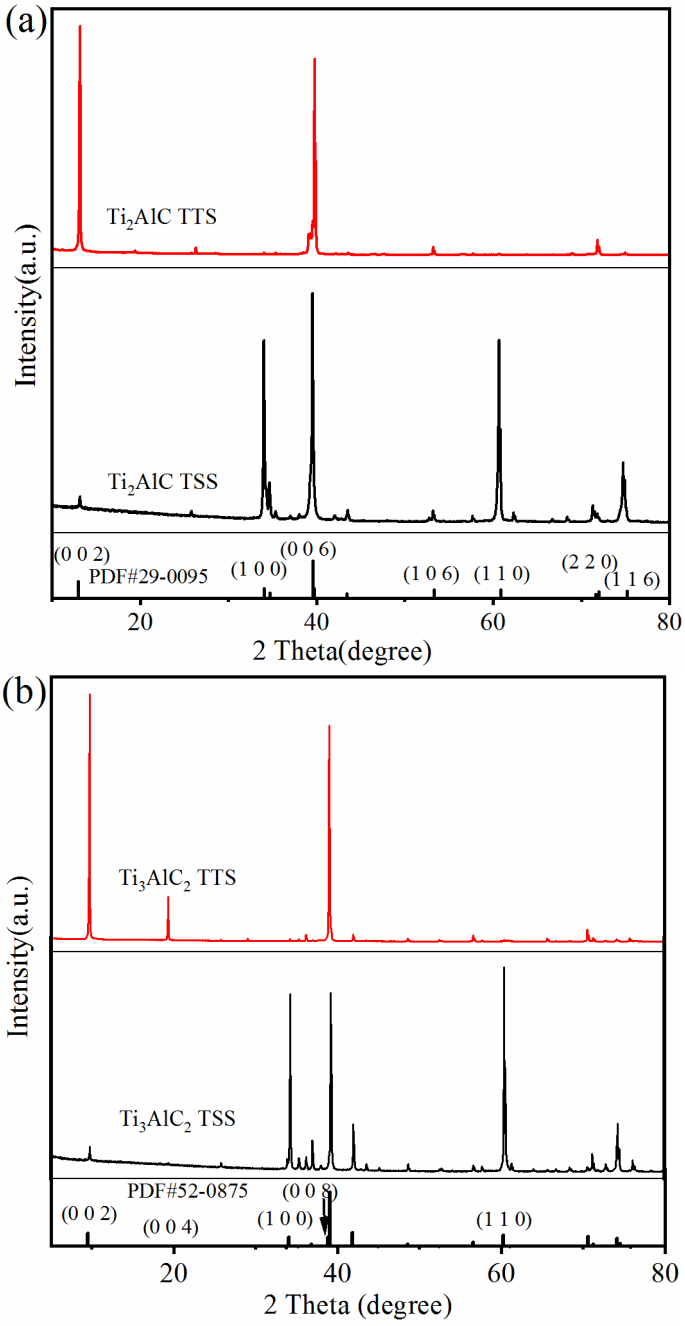

Fig. 3 The XRD patterns of textured (a) Ti_2AlC and (b) Ti_3AlC_2 ceramics.

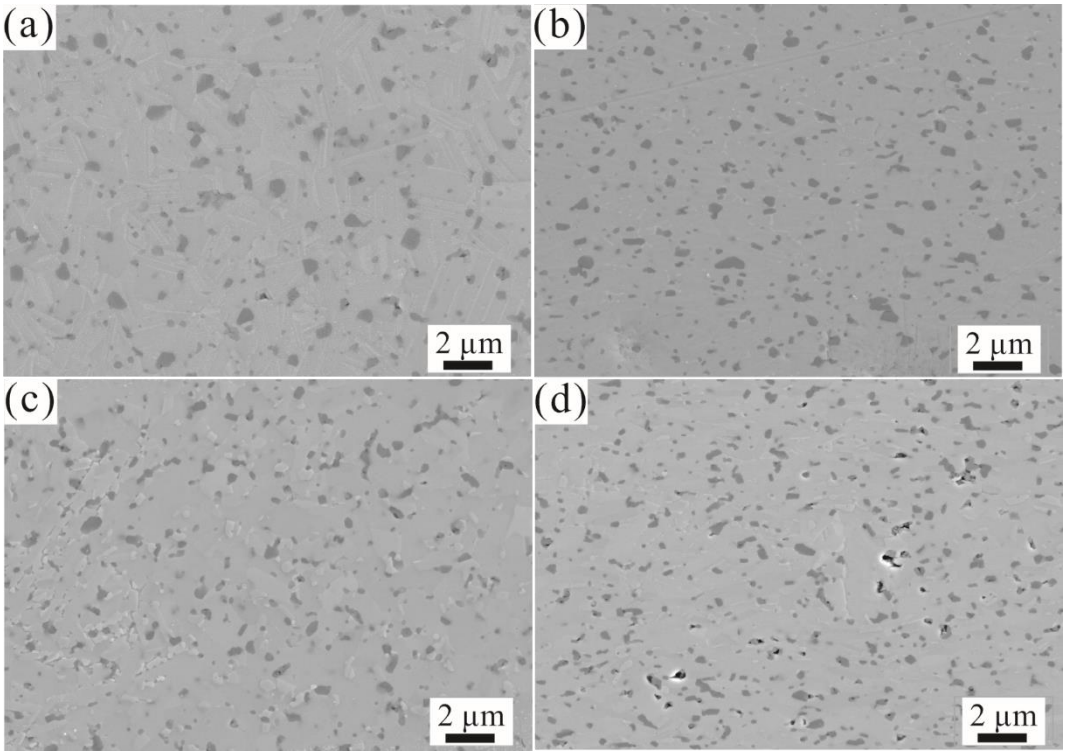

Fig. 4 SEM micrographs of polished surfaces of textured Ti_2AlC ceramic on (a) TTS; (b) TSS and textured Ti_3AlC_2 ceramic on (c) TTS and (d) TSS.

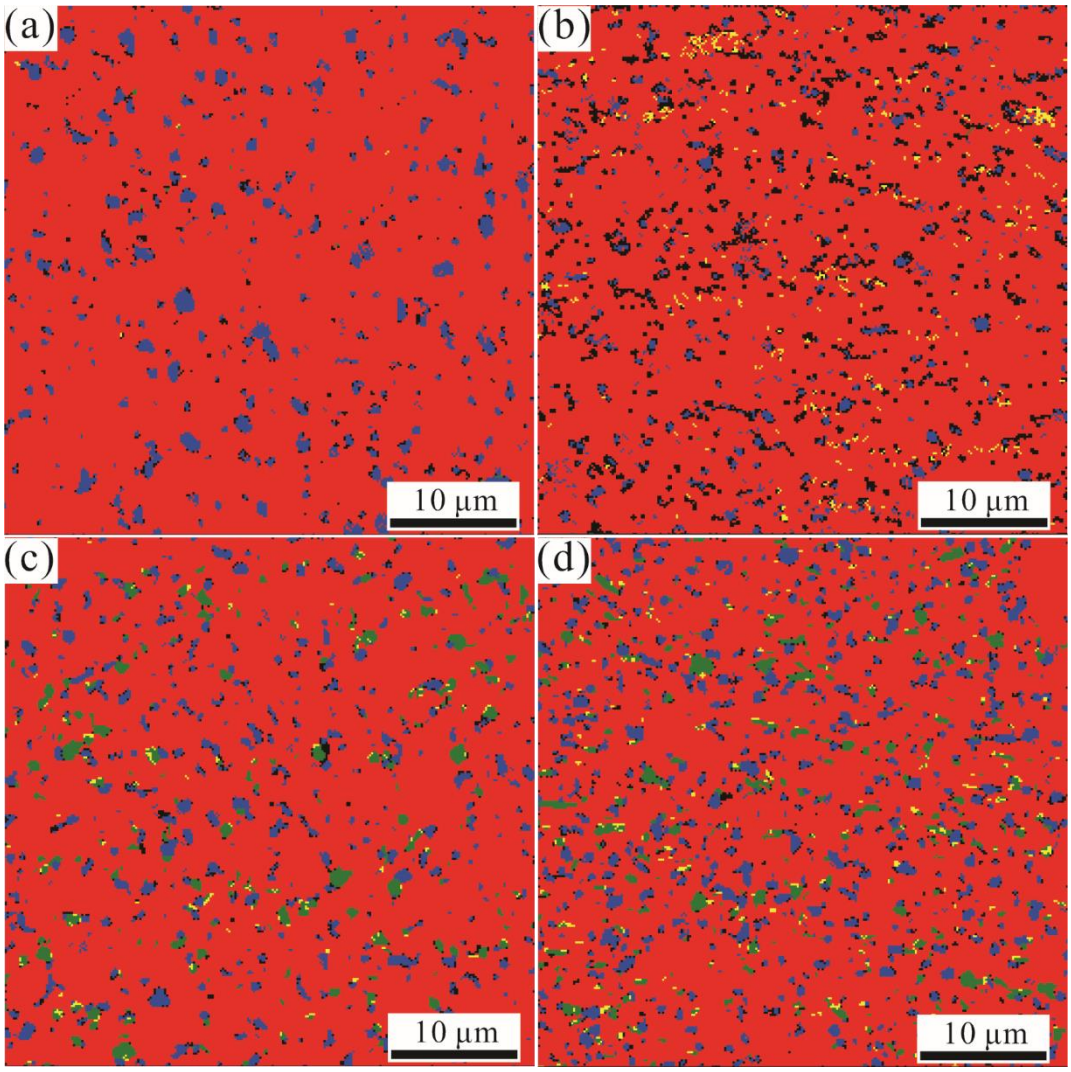

Fig. 5 The phase map of textured Ti_2AlC ceramic (a)TTS;(b)TSS and Ti_3AlC_2 ceramic (c)TTS and (d)TSS (red: Ti_2AlC, blue: Al_2O_3, yellow: TiAl, green: TiC).

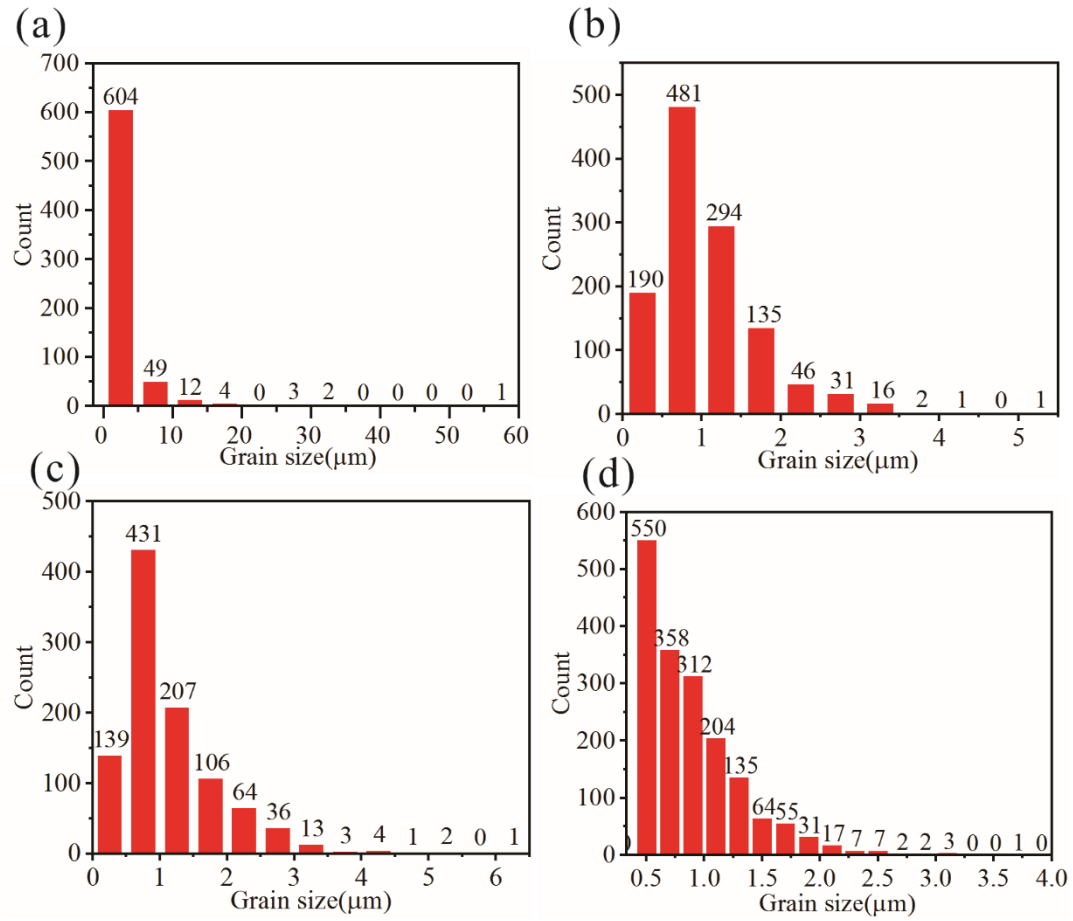

Fig. 6 The grain size of texutured Ti_2AlC (a) TTS; (b) TSS and Ti_3AlC_2 (c) TTS; (d) TSS.

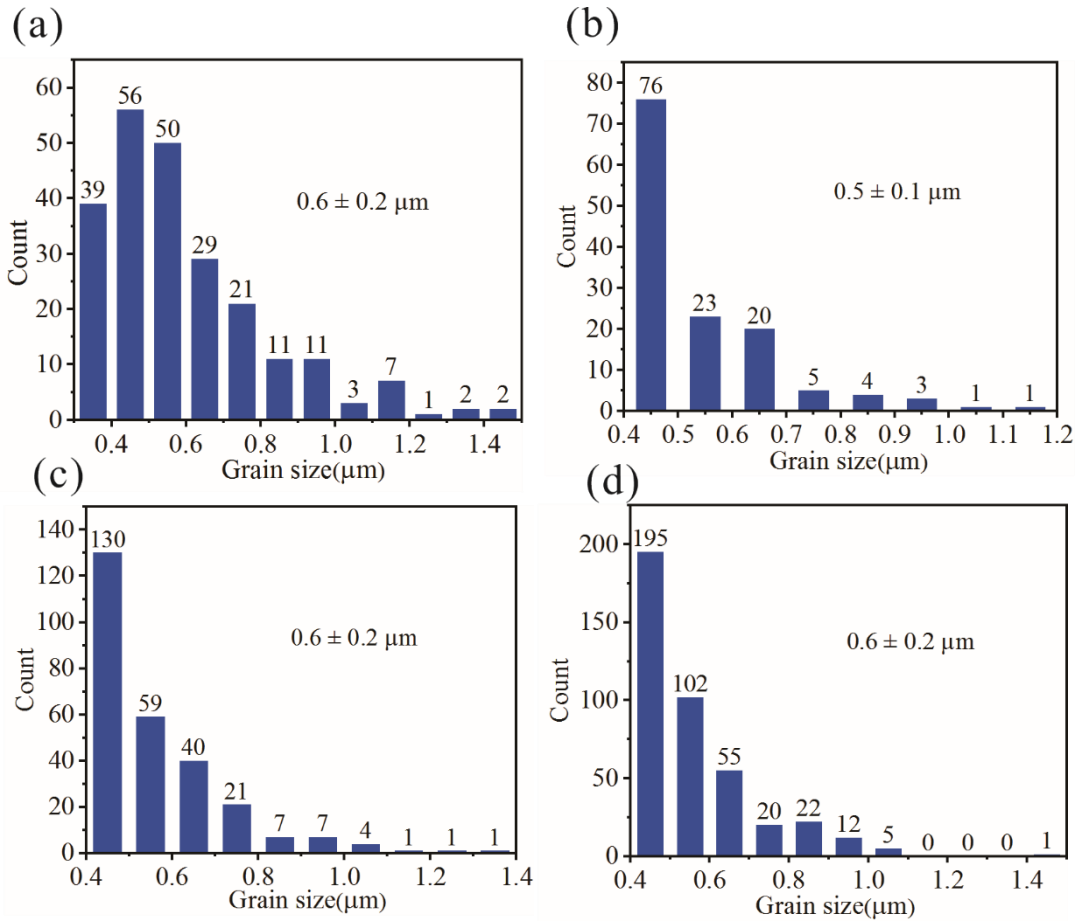

Fig. 7 The grain size of Al_2O_3 for texutured Ti_2AlC (a) TTS; (b) TSS and Ti_3AlC_2 (c) TTS; (d) TSS.

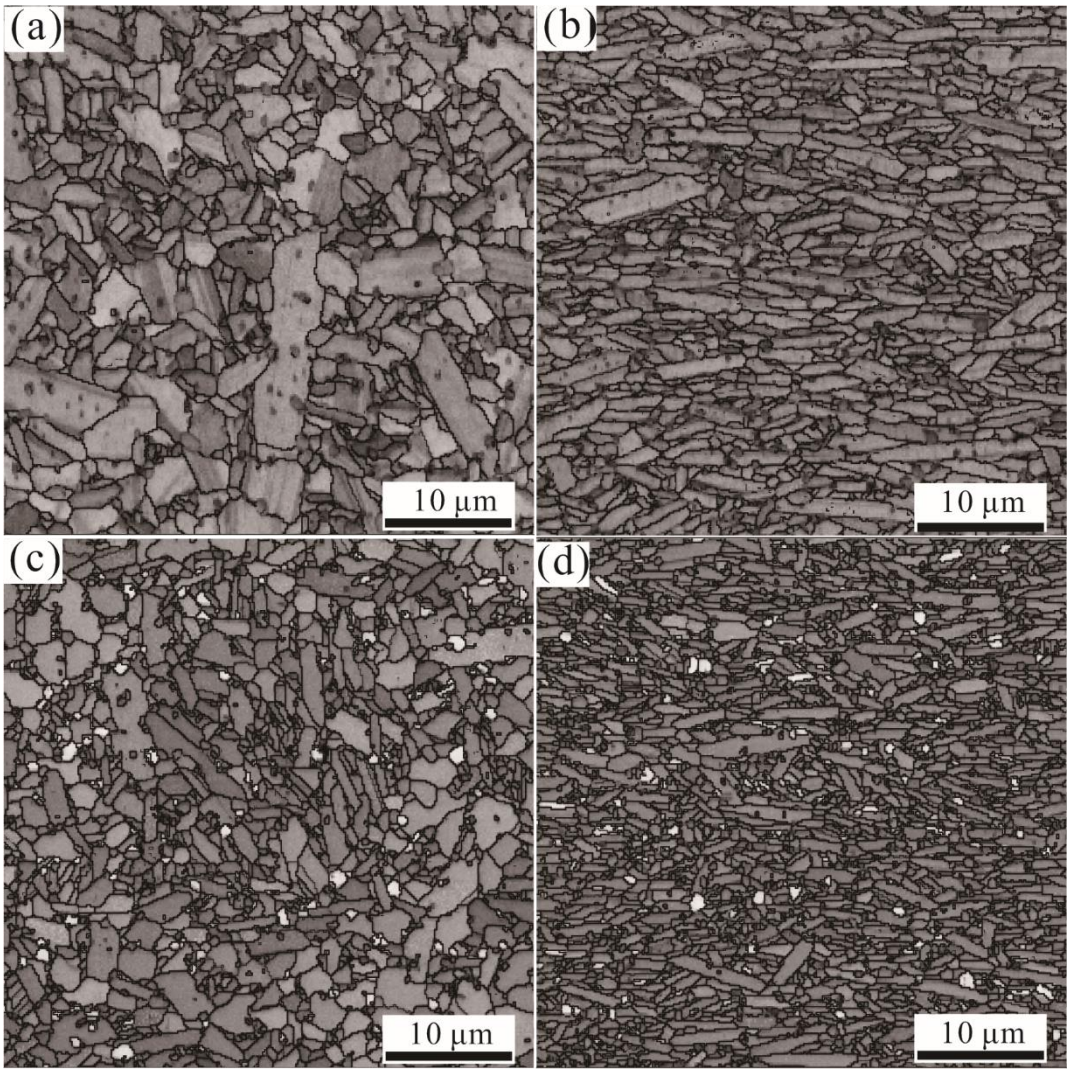

Fig. 8 The SEM images with band contrast and grain boundary of polished surfaces of textured Ti_2AlC (a) TTS;(b) TSS and Ti_3AlC_2 (c) TTS and (d) TSS.

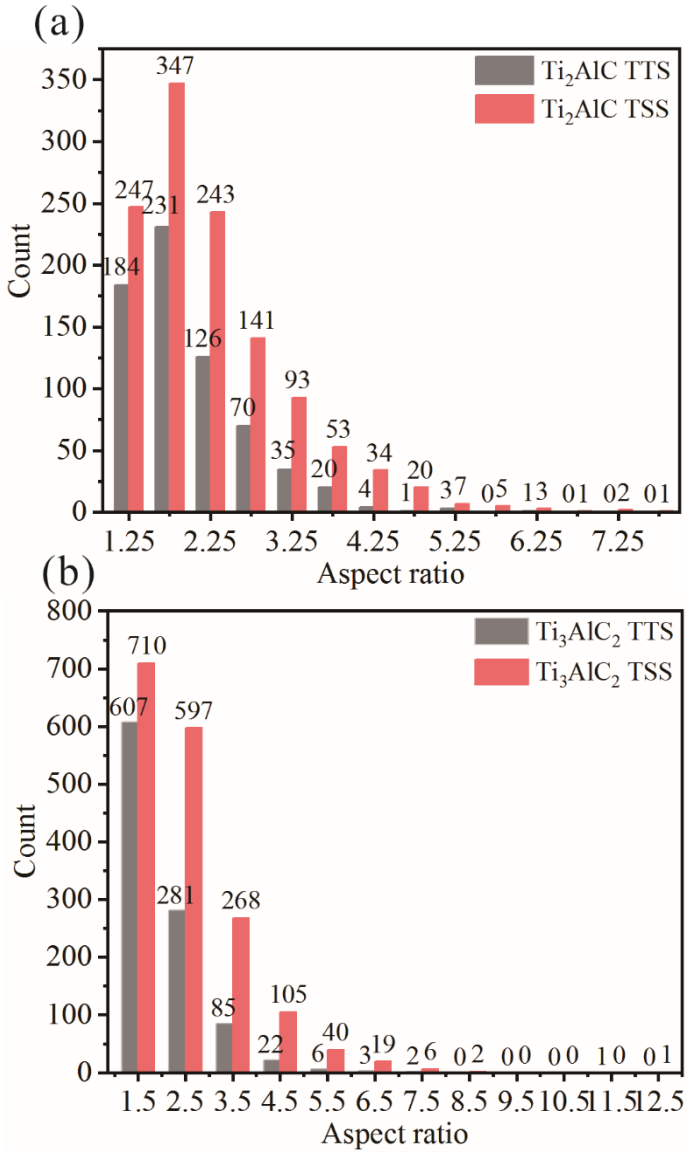

Fig. 9 The aspect ratio of textured (a)Ti_2AlC and (b) Ti_3AlC_2 ceramics.

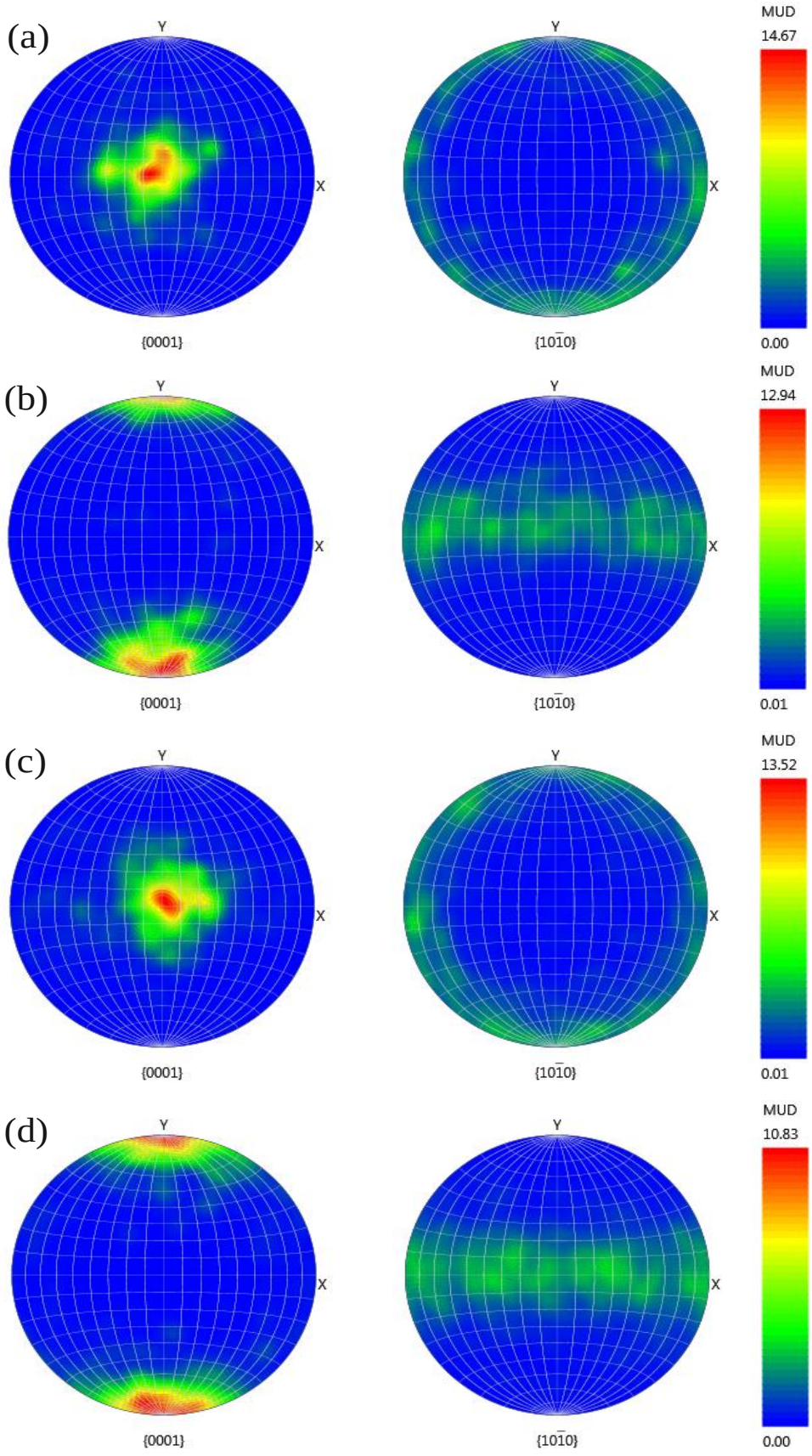

Fig. 10 The pole figure for textured Ti_2AlC (a) TTS; (b) TSS and Ti_3AlC_2 ceramics (c) TTS and (d) TSS (contour plot).

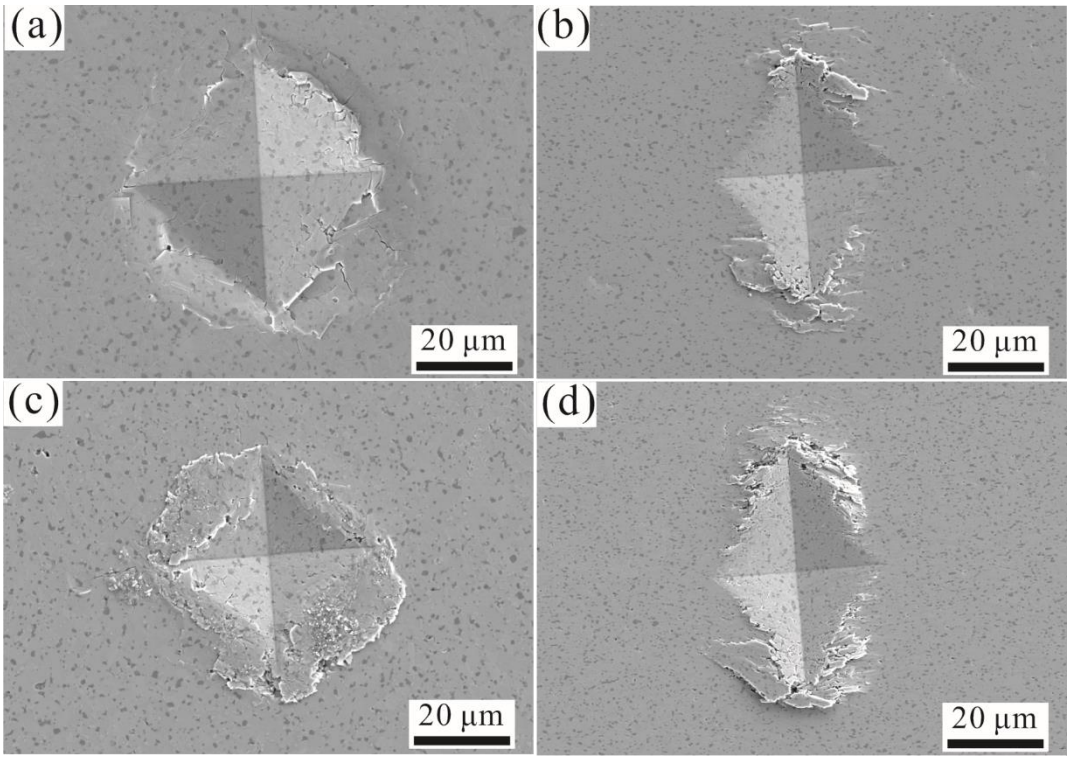

Fig. 11 The Vickers imprints at the load of 10 N for textured Ti_2AlC on (a) TTS;(b) TSS; for Ti_3AlC_2 on (c) TTS and (d) TSS.

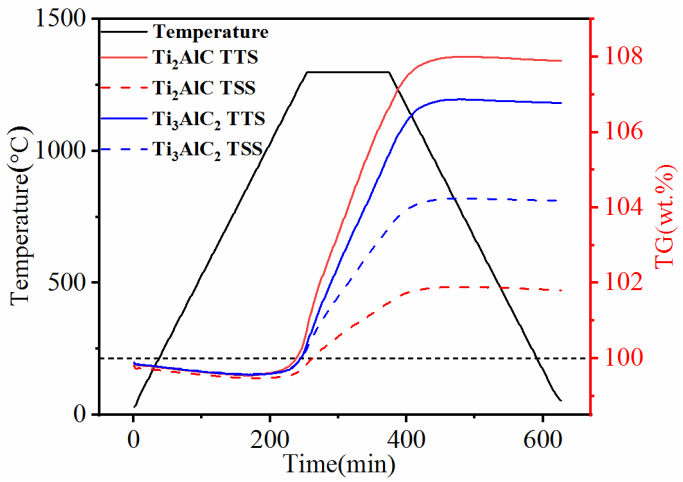

Fig. 12 The thermogravimetric analysis curve of textured carbide MAX phase ceramics.

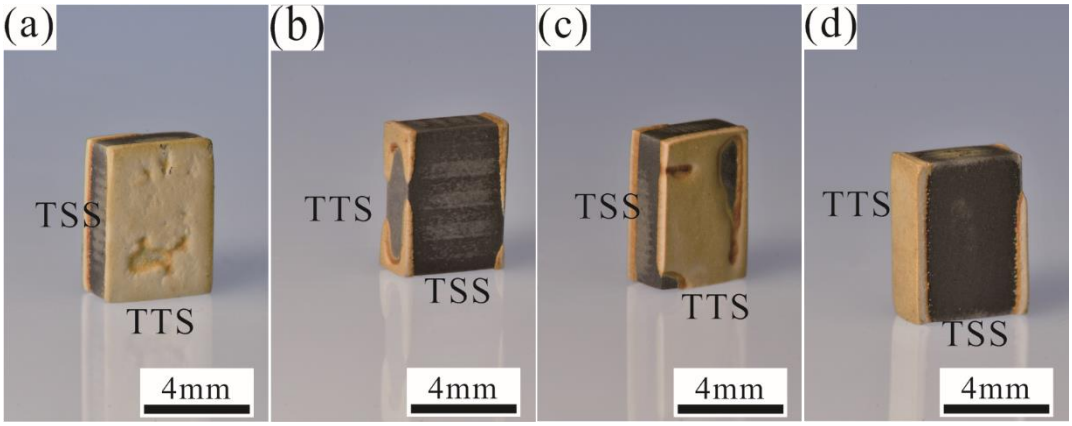

Fig. 13 The optical photographs of the oxidized textured Ti_2AlC (a)TTS-type; (b)TSS-type sample; Ti_3AlC_2 ceramics (c)TTS-type and (d)TSS-type samples after dewelling at 1300 °C for 2 h.

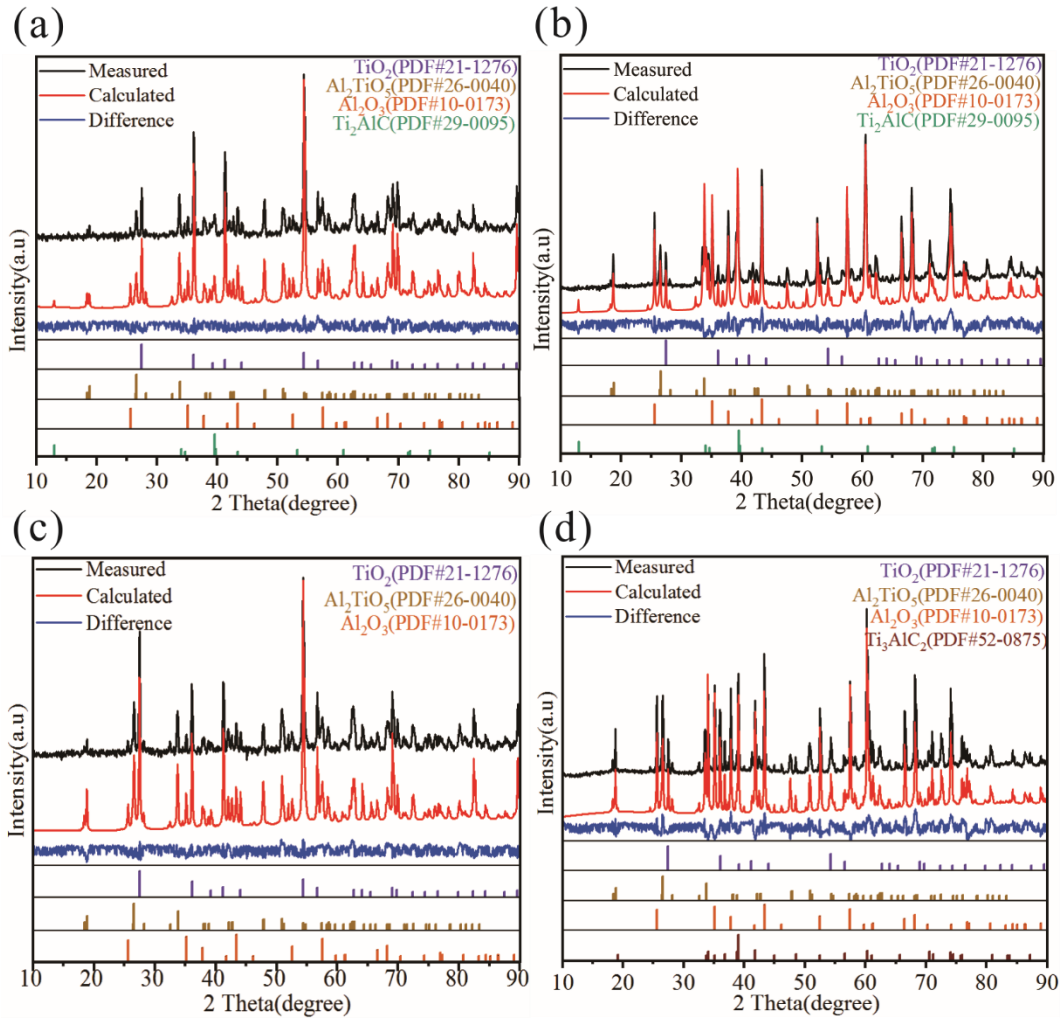

Fig. 14 The XRD patterns of oxide scale of textured Ti_2AlC on (a) TTS; (b) TSS and Ti_3AlC_2 on (c) TTS; (d)TSS after TG analysis.

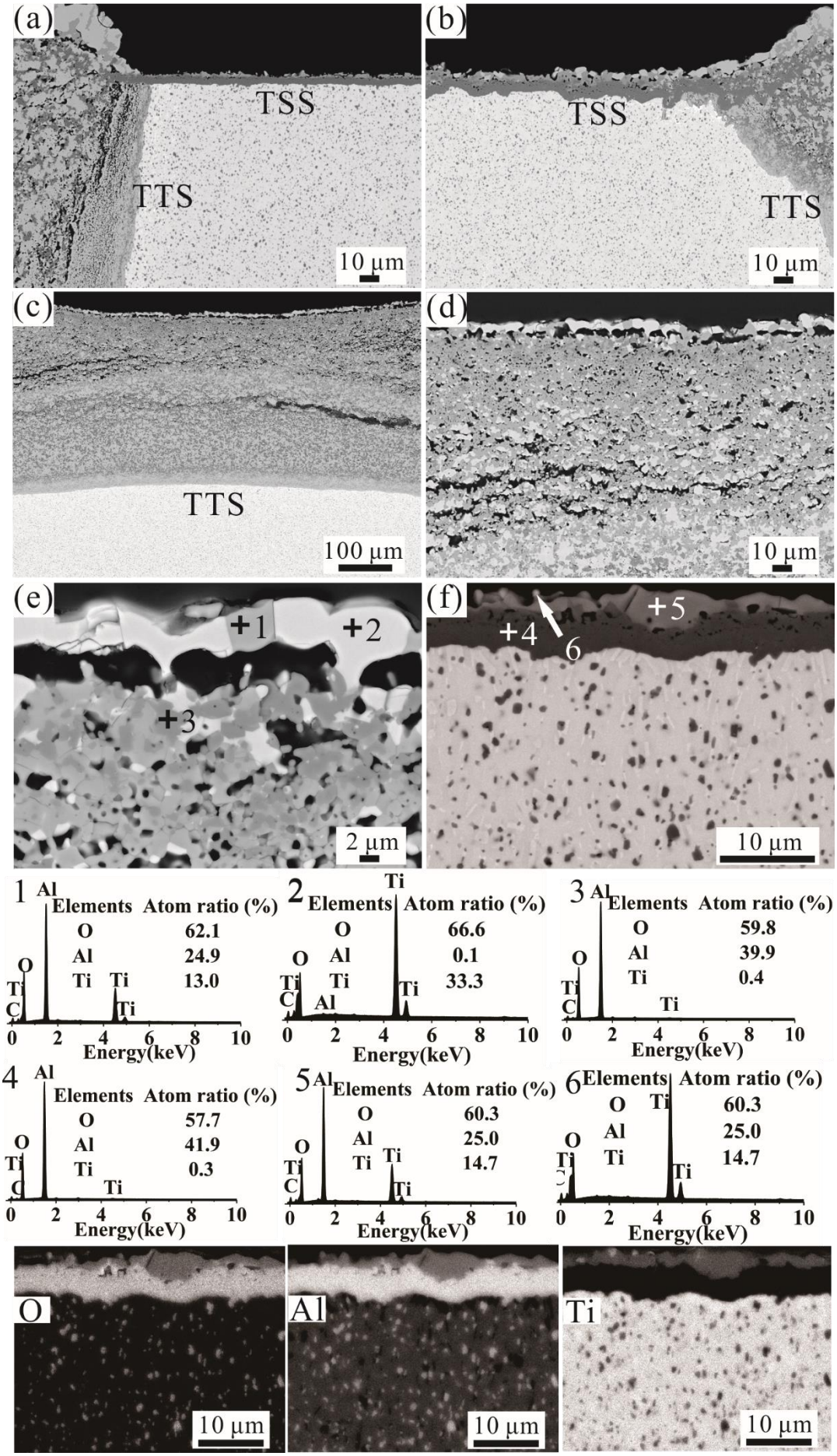
(a)
TSS
TTS
10 μm
(b)
TSS
TTS
10 μm
(c)
TTS
100 μm
(d)
10 μm
(e)
+1
+2
+3
2 μm
(f)
+4
+5
6
10 μm
1
Elements Atom ratio (%)
O 62.1
Al 24.9
Ti 13.0
2
Elements Atom ratio (%)
O 66.6
Al 0.1
Ti 33.3
3
Elements Atom ratio (%)
O 59.8
Al 39.9
Ti 0.4
4
Elements Atom ratio (%)
O 57.7
Al 41.9
Ti 0.3
5
Elements Atom ratio (%)
O 60.3
Al 25.0
Ti 14.7
6
Elements Atom ratio (%)
O 60.3
Al 25.0
Ti 14.7
Energy(keV)
O
10 μm
Al
10 μm
Ti
10 μm

Fig. 15 The SEM images of oxide scale of textured (a) Ti_2AlC; (b) Ti_3AlC_2; (c-e) on TTS of Ti_3AlC_2; (f) on TSS of Ti_3AlC_2 and corresponding EDS and elementary distribution mapping results after TG analysis.

Table 1 The amount of different phases within textured MAX phase via EBSD

Sample		The amout of different phases					Theoretical density (g/cm^3)	Relative density (%)
		Ti_2AlC	Al_2O_3	Ti_3AlC_2	TiAl	TiC		
Ti_2AlC	TTS	675	232				4.076	~100
	TSS	1197	146				4.096	99.6
Ti_3AlC_2	TTS		271	1007	4	163	4.194	99.0
	TSS		412	1748	7	194	4.189	99.1

*Theoretical densities (g/cm^3) of Ti_2AlC, Ti_3AlC_2 are 4.11 [3], 4.20 [4], respectively.

Table 2 The Vickers hardness of textured MAX phase ceramics at different loads.

Sample	Load (N)	*HV*			
		TTS		TSS	
		V_1	V_2	V	P
Ti_2AlC	1	679±34	665±28	795±30	502±20
	3	670±18	657±23	787±16	449±12
	5	665±15	630±18	775±5	440±12
	10	654±9	625±13	758±12	430±7
Ti_3AlC_2	1	768±55	749±54	815±34	473±19
	3	718±27	702±28	797±23	453±9
	5	691±23	670±23	767±16	436±7
	10	657±12	655±10	758±14	405±7

*V_1, V_2 and V represent the directions vertical to the compression direction; P represents the direction parallel to the compression direction.

Table 3 The hardness (*H*) and elastic modulus (*E*) values at different loads (mN) obtained via micro-indentation

Specimens			Load (mN)						
			10	50	100	300	500	700	1000
Ti_2AlC	*H* (GPa)	TTS	21.9 ±2.9	13.5±0.9	11.8±0.9	10.1±0.5	9.6±0.3	9.4±0.3	9.2±0.3
		TSS	18.3±1.7	11.4±0.8	10.3±0.6	10.1±0.4	9.6±0.3	9.3±0.3	9.1±0.3
	E (GPa)	TTS	270±32	260±31	256±23	237±16	229±13	223±11	213±8
		TSS	310±27	299±24	297±20	294±11	286±12	282±13	277±10
Ti_3AlC_2	*H* (GPa)	TTS	18.9±3.0	12.9±0.7	11.9±1.1	11.2±0.4	10.9±0.2	10.3±0.4	10.2±0.7
		TSS	18.7±1.6	13.0±1.2	11.6±1.2	10.4±0.7	10.3±0.4	10.2±0.5	10.1±0.5
	E (GPa)	TTS	267±21	262±18	262±16	256±15	251±11	245±14	243±14
		TSS	350±29	338±25	334±17	331±19	329±10	327±18	326±15

Table 4 Content and phase composition after oxidation on TTS and TSS sides via Rietveld analysis

Sample		Oxide products (wt. %)		
		Al_2O_3	Al_2TiO_5	TiO_2
TTS	Ti_2AlC	13	38	49
	Ti_3AlC_2	14	32	54
TSS	Ti_2AlC	73	22	5
	Ti_3AlC_2	61	35	4